THE ROLE OF THE ENDOCANNABINOID SYSTEM IN THE VASCULAR TONE

Ph.D. thesis

Bálint Bányai MD

Semmelweis University Doctoral School
Division of Theoretical and Translational Medicine

Supervisor: Eszter Mária Horváth, MD, PhD

Official reviewers: Levente Sára, MD, PhD
Olga Hajnalka Bálint MD, PhD

Head of the Complex Examination Committee:
Péter Sótonyi MD, PhD

Members of the Complex Examination Committee:
Tamás Radovits MD, PhD
Charaf Hassan Dsc. PhD

Budapest, 2025

1. Introduction

The endocannabinoid system (ECS) is a member of the endocrine system that maintains psychological balance. It primarily involves two main receptors: CB-1, mainly located in the brain, and CB-2, primarily found on peripheral areas. The system uses two main endogenous ligands, anandamide (AEA) and 2-arachidonoylglycerol (2-AG). Activation of CB–2 receptors on immune cells modulates inflammation by decreasing the production of pro-inflammatory cytokines such as TNF-α and IL-6, while increasing anti-inflammatory cytokines like IL-10. This mechanism helps reduce immune cell infiltration and tissue damage in inflammatory diseases.

Cannabinoids influence the cardiovascular system mainly through vasorelaxant effects, involving both direct actions via TRPV channels and indirect effects through PPARγ, leading to vasodilation and potential blood pressure changes. They exert their effects on the endothelium, with evidence suggesting the existence of a specific endothelial cannabinoid receptor beyond the classical CB-1 and CB-2 receptors. While CB–1 receptors are primarily involved in cardiovascular effects, CB–2 receptors play a significant role in modulating immune responses and reducing inflammation, which can benefit vascular health. In inflammatory conditions like endotoxemia and septic shock, cannabinoids, especially via CB–2, help decrease pro-inflammatory cytokines and mitigate vascular injury, contributing to their anti-inflammatory potential. Additionally, cannabinoid-based therapies show promise for managing excessive inflammatory responses such as cytokine storms, as seen in COVID-19, by regulating cytokine balance and reducing immune-mediated vascular damage.

2. Objectives

2.1. Delta-9-tetrahydrocannabinol effect on the vasorelaxation and oxidative-nitrative stress in endotoxemia

In the present study our aim was to investigate the possible beneficial effect of THC treatment on the endothelial function in a rat model of endotoxemia and its role in alterations of vascular relaxation mechanisms, and oxidative-nitrative stress.

2.2. Effect of CB-1 receptor deficiency on vascular tissue in female aorta

In our second study our aim was to identify changes in the vascular structure as well as the possibly altered presence of enzymes and receptors of vasoactive substances and oxidative-nitrative stress markers that may play role the improved endothelial function of these animals.

3. Methods

3.1. Delta 9 tetrahydrocannabinol effect on the vasorelaxation and oxidative – nitrative stress in endotoxemia

3.1.1. Animals and in vivo therapy

32 age-matched male Sprague-Dawley rats (~300 g, around 12 weeks old) were divided into three groups for a 24-hour in vivo study. The control group (n=12) received intravenous saline and intraperitoneal ethanol-saline solvent. The THC-treated group (n=8) was given 10 mg/kg THC intraperitoneally, followed 10 minutes later by 5 mg/kg intravenous lipopolysaccharide (LPS). The LPS treated group (n=12) received only LPS intravenously. After LPS administration, animals were monitored for 24 hours without anesthesia to avoid interference with results. At the end of the period, under deep anesthesia (60 mg/kg thiopentone sodium), blood and thoracic aorta samples were collected. All procedures followed NIH animal care guidelines and were

approved by the Semmelweis University ethics committee (590/99 Rh).

3.1.2. Myography of isolated aortic rings

The thoracic aorta was cleared from periadventitial fat and cut into 3–4 mm width rings, mounted in organ baths filled with warmed (37˚C) and oxygenated Krebs' solution. Isometric tension was measured with isometric transducers (10 cm^3 capacity, vertical training organ bath system, Experimetria Ltd. Budapest, Hungary.) A tension of 1.5 gram was applied and the rings were equilibrated for 60 minutes, followed by an epinephrine dose-response curve (10^{-10}–$3*10^{-6}$ M) and, after a 30- to 60-minute-long washout period, the rings were precontracted with epinephrine (10^{-7} M) and concentration-dependent relaxation to acetylcholine (Ach, 10^{-9} to $3*10^{-4}$ M) was measured.

3.1.3. Immunohistochemistry

Immunohistochemical analyses were performed on paraformaldehyde-fixed, paraffin-embedded thoracic aortic sections to assess the expression of poly(ADP-ribose) polymers (PAR), cannabinoid receptor 1 (CB-1R), cannabinoid receptor 2 (CB–2R), cyclooxygenase-2 (COX-2), endothelial nitric oxide synthase (eNOS), 4-hydroxynonenal (HNE), cyclic guanosine monophosphate (cGMP) and 3-nitrotyrosine (NT). Primary antibodies and their suppliers were as follows: monoclonal mouse anti-PAR (Abcam), monoclonal mouse anti-eNOS (Abcam), polyclonal rabbit anti-COX-2 (Abcam), polyclonal rabbit anti-HNE (Abcam), polyclonal rabbit anti-CB-1R (Cayman Chemical), polyclonal rabbit anti-CB-2R (Fabgennix), and polyclonal rabbit anti-cGMP and anti-NT (Merck Millipore). After deparaffinization, antigen retrieval was carried out in citrate buffer at pH 3 for PAR and CB–2R and at pH 6 for CB–1R, COX–2, eNOS and HNE; no retrieval step was applied for cGMP or NT. Endogenous peroxidase activity was quenched with 3 % H_2O_2 and nonspecific binding blocked with

2.5 % normal horse serum (Vector Biolabs). Sections were incubated overnight at 4 °C with primary antibodies, followed by horseradish peroxidase–conjugated anti-mouse or anti-rabbit secondary antibodies (Vector Biolabs). Signal development employed diaminobenzidine (DAB) with hematoxylin counterstaining (Vector Biolabs), and images were acquired using a Nikon Eclipse Ni-U microscope.

Quantitative assessment was conducted in ImageJ by calculating the DAB-positive area as a percentage of total tissue area: eNOS and COX–2 in the endothelium; CB–1R, HNE, NT and cGMP in the medial layer; and nuclear PAR positivity as the proportion of stained nuclei in the media.

3.1.4. Statistical analysis

Data are presented as mean ± SEM. Group differences were evaluated using or the Kruskal–Wallis test with Dunn's post hoc test for non-Gaussian data. Statistical significance was defined as $p < 0.05$. Analyses were performed by GraphPad Prism 9.5.0.

3.2. CB-1 receptor deficiency in aorta of female mice

3.2.1. Animals

Female 4–6-month-old, 20–23 g CB–1R-knockout mice (CB–1R–/–; n=25) and wild-type controls (CB–1R+/+; n=35) were studied. Animals were anesthetized with pentobarbital (Euthasol, ASTfarma; 50 mg/kg IP, plus 5–10 mg/kg as needed), perfused via the left ventricle with saline, and upper abdominal aorta segments collected for immunohistochemistry. All procedures complied with the NIH Guide for the Care and Use of Laboratory Animals (8th ed., 2011), institutional and national regulations, and were approved by the Semmelweis University Animal Care Committee and Hungarian authorities (No. PE/EA/1428-7/2018).

3.2.2. Histological and Immunohistochemical stainings

Abdominal aortic segments were fixed in 4% PFA, paraffin-embedded, and cut at 7 μm. Hematoxylin–eosin staining

(Hematoxylin Gill II, Sigma-Aldrich; Eosin Y, Merck Millipore) was used to assess intima–media ratio and wall thickness,

Immunohistochemistry targeted, eNOS (Abcam), COX-2 (Abcam), TP receptor (MyBioSource). After deparaffinization, antigen retrieval in citrate buffer (pH 6) was applied for eNOS, COX-2. Endogenous peroxidase activity was blocked with 3% H_2O_2 and nonspecific labelling of the secundary antibody was blocked with 2.5% normal horse serum (Vector Biolabs). Sections were incubated overnight at 4 °C with primary antibodies, followed by HRP-linked anti-mouse or anti-rabbit secondaries (Vector Biolabs). Staining was developed with DAB (Vector Biolabs) and counterstained with hematoxylin. Imaging was performed on a Nikon Eclipse Ni-U microscope (10× for HE, and most IHC; 20× for eNOS, COX-2).

Wall thickness and intima/media measurements were made on HE sections. Immunostaining intensity (brown DAB signal) was quantified in FIJI: eNOS and COX-2 in the endothelium; TP, in the media.

3.2.3. Statistical analysis

Results were tested with unpaired t-test. Values were expressed as mean ± standard error of mean (mean ± SEM), significance threshold was set at $p < 0.05$, Analysis was performed by GraphPad PRISM 9.5.0. (San Diego, CA, USA).

4. Results

4.1 Delta 9 tetrahydrocannabinol effect on the vasorelaxation and oxidative – nitrative stress in endotoxemia

4.1.1. Vascular functions

Following epinephrine (10^{-7} M) precontraction, applying 10^{-9} to 10^{-5} M concentrations of acetylcholine (Ach) led to arterial relaxation that was much lower in the LPS group than in the control vessels. While the LPS+THC group did not show significant differences compared to the control group above 10^{-7} M Ach concentration, so THC co-treatment was able to prevent the LPS induced endothelial dysfunction.

4.1.2. Vasoactive markers

LPS alone did not alter endothelial eNOS density, but LPS+THC significantly reduced it versus controls. COX-2 followed the same trend, with LPS+THC. Both LPS and LPS+THC groups showed marked cGMP decreases (See Figure 1).

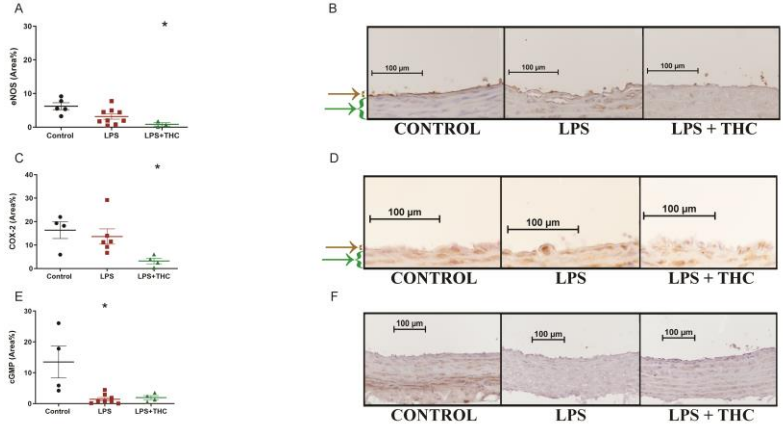

Figure 1. Histological changes of the vasoactive markers in the thoracic aorta Panel (A) endothelial NO-synthase density of the aorta's endothelial layer. Data shows positive area % of area of the endothelial layer as mean

±SEM n = 5 in Control —9 in LPS —3 in LPS+THC groups *:p<0.05 vs. Control. **Panel (B)** Representative images of eNOS stained aorta segments focusing on the endothelial layer. Brown arrows shows the intima layer, and green arrows shows the media layer of the vessels. **Panel (C)** COX—2 density in the aorta segments. Data shows positive area % of the area of the endothelial layer as mean ±SEM; N = 4(Control) —6(LPS) —4(LPS+THC) *:p<0.05 vs. Control. **Panel (D)** Representative images of COX-2 labelled aorta segments in the endothelial layer. Brown arrows shows the intima layer, and green arrows shows the media layer of the vessels. **Panel (E)** cGMP density of the aorta segments. Data shows positive area % of the total aortic tissue area as mean ±SEM; N = 4(Control) —7(LPS) —4(LPS+THC) *:p<0.05 vs. Control LPS. **Panel (F)** Representative images of cGMP labelled aorta segments. Panels B., D. and F.: Brown precipitate (3' diaminobenzidine) represents positive staining with blue hematoxylin counterstaining. Photos were taken with 20x magnification in case of eNOS and COX-2 representative photos, cropped to focus to the endothelial layer, while 10x magnification in case of cGMP representative photos focus to the media layer. In all cases statistical analysis were made using Kruskal-Wallis test and Dunn's post-hoc test.

4.1.3. Oxidative- nitrative stress status

Tissue oxidative stress was assessed by HNE staining on aortic samples. LPS raised ventricular HNE optical density, changes were not seen in LPS+THC rats. In the aortic wall, LPS also increased NT staining and PAR nuclear labeling. THC prevented the PAR rise and even lowered NT below LPS levels (See Figure 2).

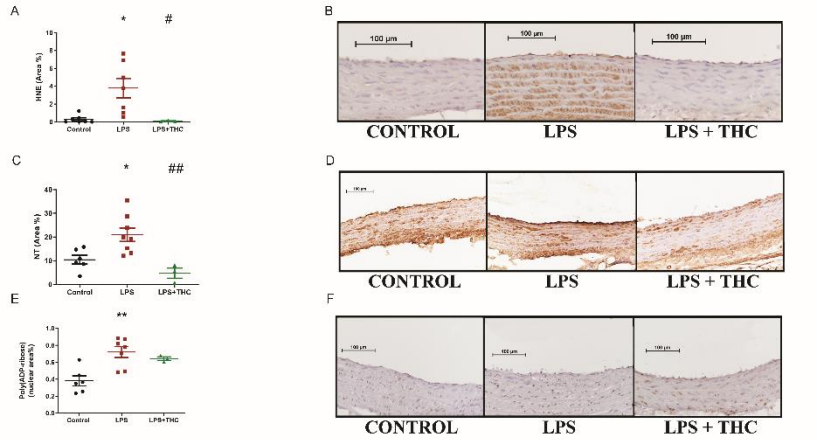

Figure 2. Oxidative- nitrative stress markers Panel (A) 4-hydroxy-nonenal staining (positive area%, n = 7–7–3) in the thoracic aortic wall showed a significant elevation in the LPS group, but not in LPS+THC animals. *p<0.05 vs. Control, #p<0.05 vs. LPS. **Panel (B)** Representative images of the aortae stained against HNE. **Panel (C)** Assessing nitrative stress. 3-nitrotyrosine (NT, positive area%, n = 6–8–3) in the thoracic aortic wall showed a significant elevation in LPS group, but not in LPS+THC animals. *p<0.05 vs. Control, ##p<0.01 vs. LPS. **Panel (D)** Representative images of the aortae stained against NT. **Panel (E)** DNA damage assessed by Poly(ADP-ribose) polymer nuclear density (PAR, positive nuclear area%, n = 6–7–3) in the thoracic aortic wall showed a significant elevation in LPS group, but not in LPS+THC animals. **p<0.01vs. Control. **Panel (F)** Representative images of the aortae stained against PAR. Panels B., D. and F.: Brown precipitate (3,3' diaminobenzidine) represents positive staining with violet hematoxilyn counterstaining. Photos were taken with 10x magnification – in case of HNE staining photos cropped to focus on the media layer. In all cases statistical analysis was executed with Kruskal-Wallis test & Dunn's post-hoc test.

4.2 CB-1 receptor deficiency in aorta of female mice

4.2.1. Vascular remodeling

The intima–media ratio showed a significant decrease in the CB–1R KO group (n = 10) in comparison to the control group (n = 6) as a result of the media layer thickening. The wall's overall thickness was increased as well. Stainings of α–smooth

muscle actin (α–SMA) did not reveal any noticeable difference between the CB–1R KO and the WT group (See Figure 3).

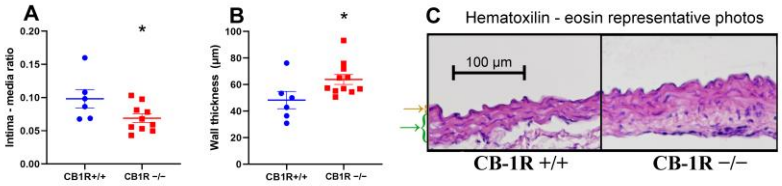

Figure 3. Morphological changes of the abdominal aorta wall Panel (**A**). Intima–media ratio of the aorta walls as mean ± SEM, n = 6 (CB–1R+/+) n = 10 (CB–1R-/-) *: $p < 0.05$ CB–1R+/+ vs. CB–1R-/- group. **Panel** (**B**). Aorta wall thickness in micrometer as mean ± SEM n = 6 (CB–1R+/+) n = 11 (CB–1R-/-) *: $p < 0.05$ CB–1R+/+ vs. CB–1R-/- group. **Panel** (**C**). Representative images of the hematoxylin-eosin staining photographed at 10x magnification. Brown arrows shows the intima layer, and green arrows shows the media layer of the vessels.

4.2.2. Vascular function

CB–1R knockout (CB–1R KO) mice showed higher aortic eNOS density than controls (Figure. 4A,B). Endothelial COX-2 expression differed between CB–1R KO and control groups (Figure. 4C,D). No TP receptor density changes were found (n=13 vs. n=6; Fig. 8E,F).

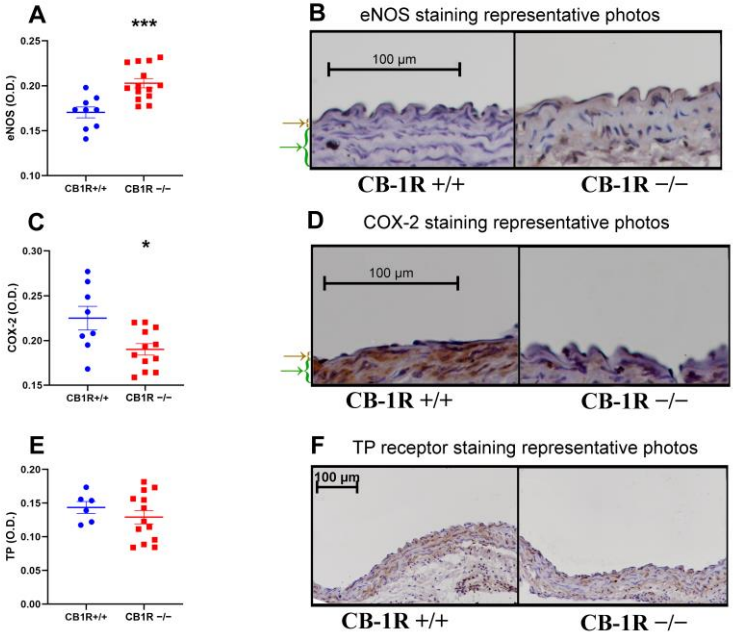

Figure 4. Vasoactive markers of the abdominal aorta wall Panel (A). Results of eNOS immunostained sections. $n = 9$ (CB–1R+/+) $n = 14$ (CB–1R-/-). ***: $p < 0.001$ CB–1R+/+ vs CB–1R-/- group. **Panel (B).** Representative images of eNOS immunostained aorta segments photographed at 20× magnification. Evaluation performed from the values of the endothelial layer. Brown arrows shows the intima layer, and green arrows shows the media layer of the vessels. **Panel (C).** Results of COX–2 immunostained sections. $n = 8$ (CB–1R+/+), $n = 12$ (CB–1R-/-). *: $p < 0{,}05$ CB–1R+/+ vs. CB–1R-/- group. **Panel (D).** Representative images of COX–2 immunostained aorta segments, photographed by 20× magnification. Evaluation performed from the values of the endothelial layer. Brown arrows shows the intima layer, and green arrows shows the media layer of the vessels. **Panel (E).** Results of TP receptor immunostained sections. $n = 6$ (CB–1R+/+), $n = 13$ (CB□1R-/-). **Panel (F).** Representative photos of TP receptor immunostained aorta segments, visualization with DAB on hematoxylin counterstaining, photographed by 10× magnification. Evaluation performed from the values of the media layer. Statistical analysis performed with unpaired *t*-test. Data shown as non–calibrated optical density with mean ± SEM.

5. Conclusions

1. Δ^9-tetrahydrocannabinol improved endothelial vascular function and oxidative-nitrative stress in endotoxemic rats.

a.) THC treatment prevented endotoxemia induced endothel dysfunction.

THC treatment was effective in rescuing endothelial dysfunction caused by endotoxemia, so that Ach-dependent relaxation was significantly improved by THC treatment in LPS treated rats.

b.) The THC-treated rats' O/N stress markers were lower than in the LPS treated group and they did not differ from the control group.

The anti-inflammatory effects of THC were also exerted - oxidative - nitrative stress levels were also significantly reduced.

All these results lead us to conclude that THC or a similar phyto/exocannabinoid analogue offers favorable therapeutic options to reverse vascular damage in endotoxemia cases.

2. CB–1 receptor deficiency vessel morphological differences.

a.) The abdominal aorta wall thickness significantly elevated while the intima media ratio decreased in the CB–1R$^{-/-}$ female mice, as we detected a significant media thickness elevation.

b.) In the CB–1R$^{-/-}$ group, the density of enzymes contributing to relaxation in the vascular endothelium also changed: eNOS density increased, while COX–2 levels decreased.

c.) ER-α density did not differ but the ER-β density significantly decreased in the CB–1R$^{-/-}$ group.

Based on these results we conclude that the favorable changes in nitric oxide and vasoactive prostanoid production together with morphological changes may contribute to an improved balance between vasoconstrictor and dilatory mechanisms.

6. Bibliography of the candidate's publications

Publications related to the thesis:

1. Banyai B, Repas C, Miklos Z, Johnsen J, Horvath EM, Benko R. Delta 9-tetrahydrocannabinol conserves cardiovascular functions in a rat model of endotoxemia: Involvement of endothelial molecular mechanisms and oxidative-nitrative stress. PLoS One. 2023;18(6):e0287168.

IF: 3.7

2. Banyai B, Vass Z, Kiss S, Balogh A, Brandhuber D, Karvaly G, et al. Role of CB1 Cannabinoid Receptors in Vascular Responses and Vascular Remodeling of the Aorta in Female Mice. Int J Mol Sci. 2023;24(22).

IF: 4.9

Combined impact factor: 8.6

Publications not related to the thesis:

3. Sziva RE, Kollarics R, Pal E, Banyai B, Korsos-Novak A, Fontanyi Z, et al. Increased Oxidative and Nitrative Stress and Decreased Sex Steroid Relaxation in a Vitamin D-Deficient Hyperandrogenic Rodent Model-And a Validation of the Polycystic Ovary Syndrome Model. Nutrients. 2025;17(2).

IF: 5.0

4. Vass Z, Shenker-Horvath K, Banyai B, Veto KN, Torok V, Gem JB, et al. Investigating the Role of Cannabinoid Type 1 Receptors in Vascular Function and Remodeling in a Hypercholesterolemic Mouse Model with Low-Density Lipoprotein-Cannabinoid Type 1 Receptor Double Knockout Animals. Int J Mol Sci. 2024;25(17).

IF: 4.9

5. Suli A, Magyar P, Vezer M, Banyai B, Szekeres M, Sipos M, et al. Effects of Gender and Vitamin D on Vascular Reactivity of the Carotid Artery on a Testosterone-Induced PCOS Model. Int J Mol Sci. 2023;24(23).

IF: 4.9

6. Bencsics M, Banyai B, Ke H, Csepanyi-Komi R, Sasvari P, Dantzer F, et al. PARP2 downregulation in T cells ameliorates lipopolysaccharide-induced inflammation of the large intestine. Front Immunol. 2023;14:1135410.
IF: 5.7
7. Vezer M, Josvai A, Banyai B, Acs N, Keszthelyi M, Soltesz-Katona E, et al. Impact of Sex and Exercise on Femoral Artery Function: More Favorable Adaptation in Male Rats. Life (Basel). 2023;13(3).
IF: 3.2
8. Vezer M, Demeter A, Szekeres M, Josvai A, Banyai B, Olah A, et al. Sex differences in rat renal arterial responses following exercise training. Am J Physiol Heart Circ Physiol. 2022;322(2):H310-H8.
IF: 4.8
9. Tarszabo R, Banyai B, Ruisanchez E, Peterffy B, Korsos-Novak A, Lajtai K, et al. Influence of Vitamin D on the Vasoactive Effect of Estradiol in a Rat Model of Polycystic Ovary Syndrome. Int J Mol Sci. 2021;22(17).
IF: 6.208
10. Sipos M, Gerszi D, Dalloul H, Banyai B, Sziva RE, Kollarics R, et al. Vitamin D Deficiency and Gender Alter Vasoconstrictor and Vasodilator Reactivity in Rat Carotid Artery. Int J Mol Sci. 2021;22(15).
IF: 6.208
11. Merkely P, Bakos M, Banyai B, Monori-Kiss A, Horvath EM, Bognar J, et al. Sex Differences in Exercise-Training-Related Functional and Morphological Adaptation of Rat Gracilis Muscle Arterioles. Front Physiol. 2021;12:685664.
IF: 4.755
12. Lajtai K, Tarszabo R, Banyai B, Peterffy B, Gerszi D, Ruisanchez E, et al. Effect of Vitamin D Status on Vascular Function of the Aorta in a Rat Model of PCOS. Oxid Med Cell Longev. 2021;2021:8865979.

IF: 7.310
13. Sipos M, Peterffy B, Sziva RE, Magyar P, Hadjadj L, Banyai B, et al. Vitamin D Deficiency Cause Gender Specific Alterations of Renal Arterial Function in a Rodent Model. Nutrients. 2021;13(2).
IF: 6.706
14. Lajtai K, Nagy CT, Tarszabo R, Benko R, Hadjadj L, Sziva RE, et al. Effects of Vitamin D Deficiency on Proliferation and Autophagy of Ovarian and Liver Tissues in a Rat Model of Polycystic Ovary Syndrome. Biomolecules. 2019;9(9).
IF: 4.082
15. Gerszi D, Penyige A, Mezei Z, Sarai-Szabo B, Benko R, Banyai B, et al. Evaluation of oxidative/nitrative stress and uterine artery pulsatility index in early pregnancy. Physiol Int. 2021;107(4):479-90.
IF: 2.090
∑IF: 73,659